BUNCH-BY-BUNCH DIAGNOSTICS AT THE APS USING TIME-CORRELATED SINGLE-PHOTON COUNTING TECHNIQUES*

B. X. Yang, W. E. Norum, S. Shoaf, and J. Stevens
Advanced Photon Source, Argonne National Laboratory, Argonne, IL 60439, USA.

Abstract

Time-correlated single-photon counting (TCSPC) techniques have been used for bunch purity measurement since the Advanced Photon Source (APS) started operations. Recent improvements of the monitor have increased the signal-to-noise ratio and dynamic range to about 100 billion. Resolution improvements of commercial TCSPC components to under 50 ps FWHM allowed us to measure the longitudinal profile of individual bunches in the APS storage ring using a single-photon avalanche photodiode and a PicoHarp 300 TCSPC unit. Due to its robustness, the system operates continuously and measures the average longitudinal profile of the stored beam, updating the process variables for bunch phases and bunch lengths every 8 seconds. In a third application, using a TCSPC x-ray detector with an x-ray wire scanner in the monochromatic beam of the diagnostics undulator, measurements of transverse profiles of individual bunches can be completed in less than 4 minutes. It showed that, due to energy losses to the storage ring impedance, the high-current bunch clearly travels a different trajectory from low-current bunches. These bunch-by-bunch diagnostics provide valuable beam information to users performing timing experiments.

INTRODUCTION

Time-correlated single photon counting (TCSPC), a technique for measuring arrival time of the photon pulses against a clock pulse train, is a well-established technique for studying time-resolved phenomena in physics, chemistry and biology [1,2]. At the Advance Photon Source (APS), this technique has been used for bunch purity measurement since 1999 [3].

Figure 1 shows a conventional TCSPC instrument. It uses a time-to-amplitude converter (TAC) to produce a pulse with its amplitude proportional to the interval of time between the signal pulse (START) and the clock pulse (STOP), and an analogue-to-digital converter (ADC) to measure the pulse height. Since only one signal pulse can be processed during the interval between two clock pulses, the dead time may be as long as a clock period, and obtaining a high count rate and long time-scale at the same time is difficult. Modern TCSPC instrument, however, digitizes the event time using time-to-digital converters (TDC). Figure 2 shows the timing diagram of a TDC: A high-frequency clock and one or more lower-frequency timing signals establish a timing grid. Internally, the TDC generates higher-frequency ticks to make finer timing divisions. When a signal pulse (event) triggers the counter, the number of ticks since the last clock pulse, $\tau(k)$, the number of clock pulses since the last timing marker, $t(j)$, and the number of timing markers since the instrument are enabled, $T(i)$, are recorded by the internal circuitry, giving the complete timing information of the event. In the time-tagged time-resolved (TTTR) mode, the complete set of event timing information, (i, j, k), is recorded for user processing. In histogram mode, these events are collected and made into frequency of occurrence within designated intervals by an internal program. Using the TDC, more than one event can be recorded between two clock pulses, and a high count rate of several Mc/s is not in conflict with a long time scale of μs or even ms. In the following examples, we will show how the TDC-based TCSPC techniques are used at the APS for accelerator diagnostics.

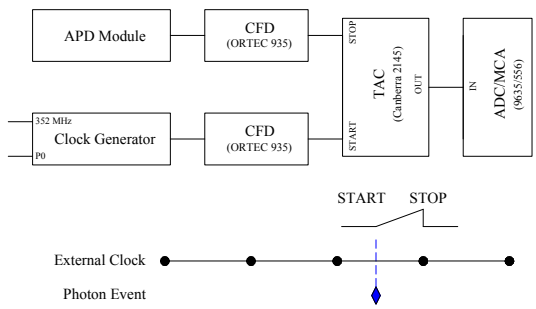

Figure 1: Conventional TCSPS and timing diagram.

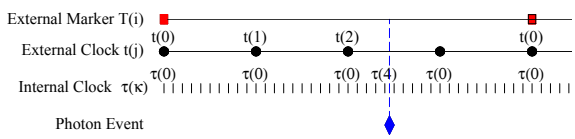

Figure 2: Digital TCSPS timing diagram.

BUNCH PURITY MONITOR UPGRADE

The original APS bunch purity monitor used the conventional TAC-ADC technique. It was used 2–3 times daily and provided bunch purity data typically at the 10^{-6} – 10^{-7} level [3]. Our upgrade effort included redesign of the fluorescence-target; improvement of the detector and analogue electronics operations, and implementation of an field-programmable gate array (FPGA) based TDC [4].

Redesign of the fluorescence target chamber

Figure 3 shows the redesigned fluorescence target

* Work supported by U.S. Department of Energy, Office of Science, Office of Basic Energy Sciences, under Contract No. DE-AC02-06CH11357

chamber. The chamber is made of thick brass alloy, which contains 3% Pb to provide effective shielding from scattered x-rays in the hutch. The target chamber is 1 cm in diameter, 2.5 cm long. The entrance path was shielded by a long, narrow tube to reduce solid angles of back-scattered x-rays. By shortening the multiple-scattering time to well below the accelerator bucket length of 2.84 ns (80 cm), we make the backscattered x-ray pulses appear under the main peak, instead of several ns later. Furthermore, the upstream white x-ray slits are opened wider to improve the signal-to-noise ratio.

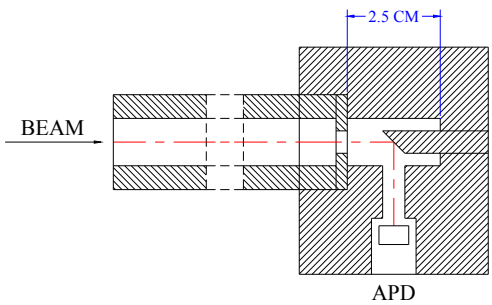

Figure 3: A compact target chamber design.

Fpga-based time-to-digital converter

A fast TDC was implemented on an Altera Stratix II fpga [4], using the storage ring revolution clock (P0) as the coarse timing marker and the 44-MHz subharmonic of the storage ring rf frequency as the external clock. Inside the fpga, the external clock frequency was quadrupled to provide a 352 MHz bunch clock; and it is further multiplied 16 times to make internal clock ticks. Due to a limitation of the FPGA, only six accumulators can be implemented per bucket, allowing 7776 accumulators per revolution of electrons in the ring. In the experiment, we found that the FPGA system may handle count rate well above 1 Mc/s while maintaining the range of 3.68 μs to cover the entire ring. However, we were unable to test the system's theoretical 176 MHz burst count rate limit. As we will see in the next paragraph, the TDC provided additional timing information for trouble-shooting the bunch purity monitor detectors and electronics.

Improved operation of detector electronics

In the old configuration, the APD detector module is connected to a constant fraction discriminator (CFD) located outside of the x-ray enclosure via a coaxial cable over 40 m long, which significantly attenuated the 2-ns signal pulse and picked up substantial rf noise from the accelerator components located nearby. To characterize the source of the noise, we moved the APD detector away from the target to reduce the signal and collected counts continuously for 5 hours. Figure 4 shows a histogram as a function of bucket numbers, where a significant level of noise can be seen between buckets Nos. 800 and 900. Figure 5 shows the integrated counts between bucket numbers 845 and 890, plotted as a function of time. We can see that the noise counts are recorded only during top-up injections when the stored current increases. We concluded that the long signal cable was picking up injection kicker pulses from the storage ring.

To reduce the noise pickup, we installed a CFD within 1 m from the APD detector module, and its threshold was set higher to match the unattenuated signal amplitude. This immediately improved the measured bunch purity to down around the 10^{-10} level, as can be seen in Figure 6. At this level, after-pulsing of the APD detector [5] appeared to be the main contributor of the background. We discovered that, if the applied high voltage on the APD is turned off for one minute every few hours and the accumulated charges are drained through a 10-Mohm resister bypassing the APD, the background counts can be significantly reduced, as shown in Figure 7. This power cycle is performed automatically by the EPICS IOC controlling the pulse processor.

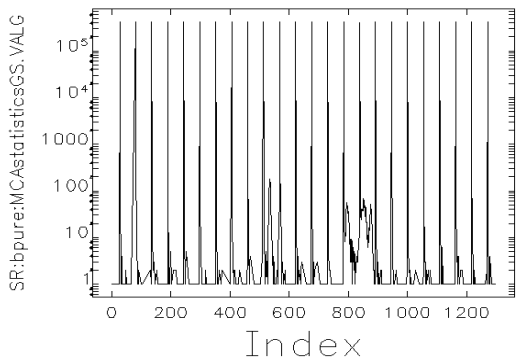

Figure 4: Noise picked up by long cables of APD module: The horizontal axis shows the rf bucket number; the vertical axis shows the counts per bucket.

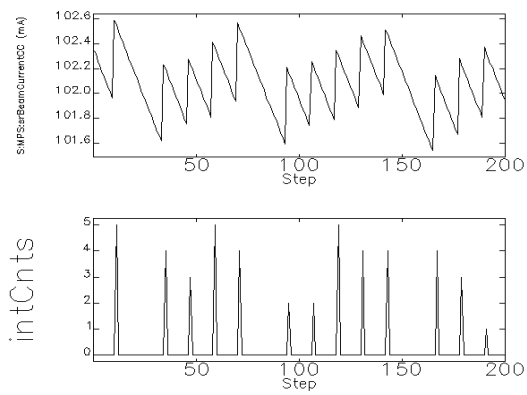

Figure 5: Integrated counts between bucket numbers 845 and 890. The bottom plot shows correlation with top-up injection as indicated by current increase in the top plot.

Figure 7 also shows a typical bunch purity histogram: while the main peak exceeds 10^{11} counts cumulated over 5 days, there are few counts between 20th and 30th buckets after the main bunch. The impurity bunch profile shows

the electron halo density in the fundamental bucket of the APS injector Particle Accumulator Ring (PAR), with more pronounced peaks at ±3 buckets due to the 12-th harmonic (117.3 MHz) rf compressor. A broad peak below 10 counts can be seen around bucket No. 36, which originates from the rare event when a few electrons are extracted in the second turn and survived through the booster synchrotron. All these impurity peaks are carefully monitored during user operations so they do not increase out of specifications.

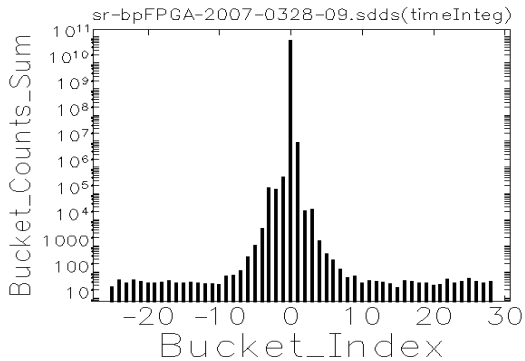

Figure 6: Bunch purity histogram using a CFD near the APD. The background is likely from afterpulsing.

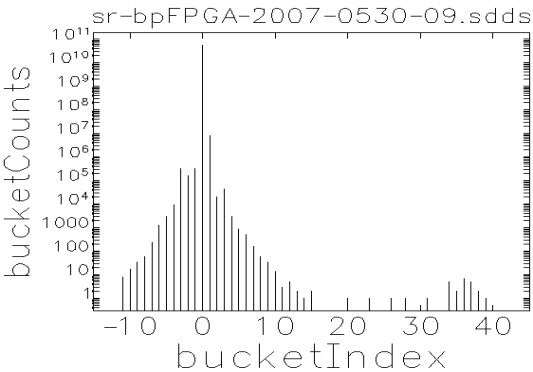

Figure 7: Bunch purity histogram with periodic automatic power cycling of the APD.

BUNCH LENGTH MONITOR

Since 1997, streak camera has been used to measure the bunch length and longitudinal bunch profiles at the APS. As users require more detailed timing information for their increasingly sophisticated experiments, a reliable diagnostics needs to be developed to continuously provide longitudinal bunch profile information. Due to our experience with the robust operation of the bunch purity monitor, the TCSPC technique became our first candidate for this bunch length monitor.

The temporal resolution of the commercial TSCPC electronics has improved continuously and reached a few ps rms in the last decade. At the same time, fast single-photon avalanche photodiodes (SPAD) with advertised time resolution better than 50 ps FWHM and maximum count rate exceeding 1 Mc/s have become commercially available. Their resolution compares favourably with the ~ 50 ps rms width of the 16-mA bunch for hybrid fill operations, and ~ 40 ps rms width of the 24-bunch normal operations of the APS storage ring. Figure 8 shows the setup of our TCSPC bunch length monitor: The visible synchrotron light is focused on an SPAD, id100-20 from IDQ [6]. The output pulse of the detector was inverted, attenuated and fed to a TCSPC pulse counter, PicoHarp 300 from PicoQuant [7], which operated in the histogram mode. When tested with two bunch clock generators, one connected to the clock input (0) and another to the event pulse input (1), the combined electronic resolution was found to be 9 ps rms. To estimate the overall system resolution, we used the short electron bunches with a bunch current ~ 0.3 mA, during the 324-bunch beam operations.

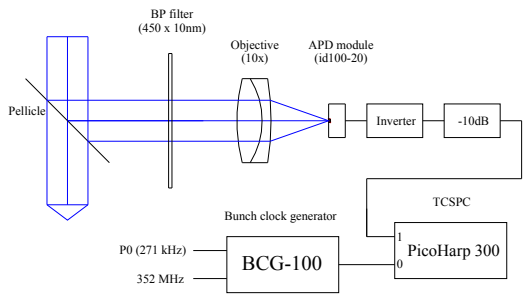

Figure 8: Schematic of the TCSPC bunch-length measurement system.

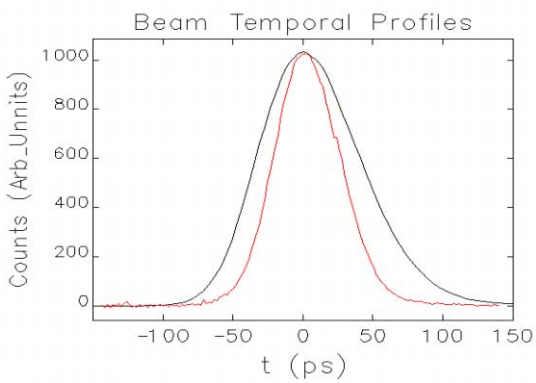

Figure 9: Acquired temporal profile for short bunches using a streak camera (red) and the TCSPC technique (black).

Figure 9 shows the temporal profiles acquired at the same time by both the TCSPC system and the streak camera. While the streak profile fits well with a Gaussian function with an rms width of 23.4 ps, the fit to the TCSPC profile gives an rms width of 35.7 ps. We concluded that the TCSPC system using id100-20 has an effective rms resolution of 27 ps, which is dominated by the contribution from the SPAD. While the short electron bunches are useful for calibration of the TCSPC system,

they are not being used by APS users for time-resolved experiments due to the short bunch spacing of 11 ns. Figure 10 shows the temporal profiles taken with TCSPC technique the using id100-20, PDM-50CT, another SPAD from Micro Photon Device [8], and a micro channel plate photomultiplier (MCP-PMT) from Hamamatsu, with a 4-mA bunch current, during 24-bunch operation. The profiles are compared with one acquired with a streak camera. While other TCSPC detectors have better resolution than the id100-20, as evidenced by the sharp front edges, their profiles contain significant tails. The figure also shows that the TCSPC profile is reasonably close to the true temporal profile of the bunch.

The histogram has 64 K channels, covering 260 ns at the highest resolution of 4 ps/bin. Since the storage ring revolution time is 3.68 μs, we need to set three clock pulses per revolution to fit all bunches in the histogram for hybrid fill, as shown in Figure 11. The bunches are, from left to right, Bucket 0 (16 mA), Groups 5, 1, 6, 2, 7, 3, 8, and 4. Each group contains seven 1.5-mA bunches.

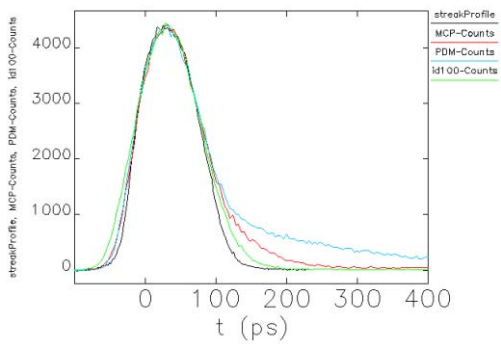

Figure 10: Comparison of the longitudinal profiles acquired with SPAD modules id100-20 (green) and PDM-50CT (blue), MCP-PMT R3809U-50 (red), and the Hamamatsu streak camera (black).

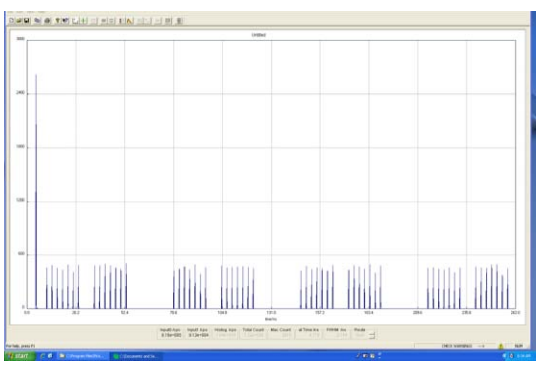

Figure 11: PicoHarp 300 control screen for profile measurement of hybrid fill.

A PC running Red Hat Enterprise Linux (RHEL) was used to control the PicoHarp through its USB interface. A histogram is accumulated every 8 seconds and transferred to the Linux PC, where it was sorted and the longitudinal time coordinates were added using the internal clock and the storage ring rf frequency at the time. The longitudinal profiles are fitted to a Gaussian function to obtain phase and width information. These profiles and fit parameters are made available online as process variables. Figure 12 shows a sample MEDM screen for the temporal profile of the 16-mA bunch during the hybrid fill operation.

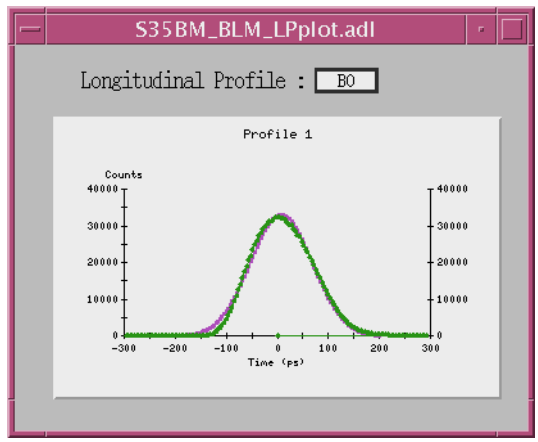

Figure 12: MEDM screen showing the acquired temporal profile of the 16-mA bunch (green) along with a Gaussian fit to the profile curve (purple).

X-RAY WIRE SCANNER

During the beam operations with hybrid fill, electron bunches with very different bunch currents are circulating in the ring at the same time. It is natural to ask whether these bunches have different energies and travel in different trajectories, and whether their differences impact user experiments. Measurement of the bunch properties can be performed using gated optical (gated camera) or electrical (BPM) detectors. However, the intensity dependence of these detectors often complicates the quantitative interpretation of the data. The TCSPC technique, while measuring only average properties, has a large dynamic range and collects data simultaneously for all bunches, significantly reducing potential ambiguities.

For a high S/N ratio, a scanning slits measurement is optimal, as shown in the discussions of the bunch purity monitor. But it also intercepts the entire beam. An x-ray wire scanner, on the other hand, minimizes its disturbance on the x-ray beam. Figure 13 shows such a scanner design. A copper wire with a diameter less than $\sigma/3$, where σ is the rms size of the x-ray beam, scans through the monochromatic x-ray beam at 30 m from the undulator source. The Cu-*K* x-ray fluorescence (XRF) photons from the wire are detected by an x-ray APD mounted nearby. A FPGA-based TCSPC pulse counter is used to determine the bunch number that excites the XRF. After completing the transverse scan, a computer program resorts the data and generates the transverse intensity profiles of individual x-ray bunches. Figures 14 and 15 show the horizontal and vertical bunch profiles, respectively for the hybrid fill pattern after normalizing them at the peaks.

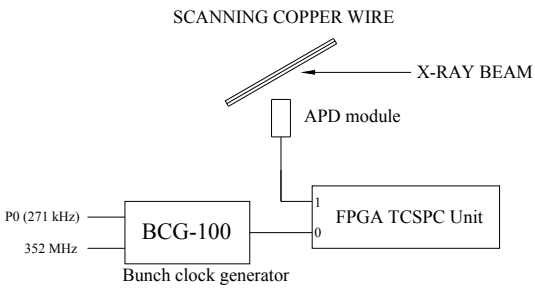

Figure 13: Schematic of the x-ray wire scanner.

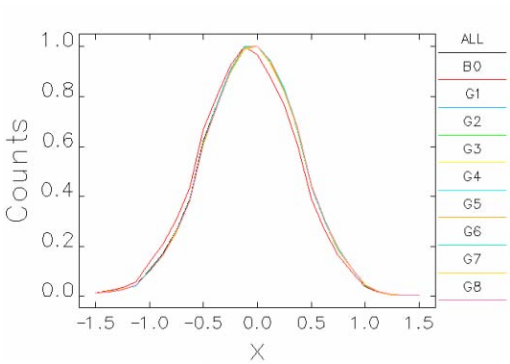

Figure 14: Normalized x-ray beam profiles for hybrid fills in the horizontal direction. The high-current bunch is offset from other low-current bunches by 50 µm.

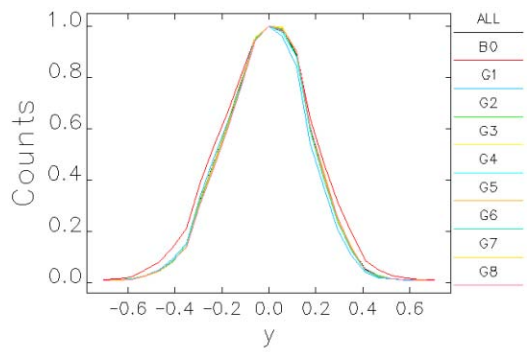

Figure 15: Normalized x-ray beam profiles for hybrid fills in the vertical direction. The high-current bunch is larger than the low-current bunches by about 20%.

Figure 14 shows that the horizontal x-ray profile of the high-current bunch is shifted by 50 µm compared to low-current bunches at 30 m from the undulator. This is likely due to the energy losses to the storage ring impedance: A high-current bunch loses more energy per turn in the storage ring. To maintain the same average energy as the low-current bunches, it acquires more energy from the rf cavity. Hence the electrons in the high-current bunch have higher energy at Sector 1 coming out of the rf cavities, and lower energy at Sector 35 before re-entering the rf cavities. As a result, the x-ray spectra of the high-current bunch are shifted higher in Sector 1 but shifted lower in Sector 35. At locations with non-zero dispersions / dispersion slopes, the x-ray source / beam directions from the high-current bunch differ from those from the low-current bunches. In Figure 4, the dispersion slope is likely the main contributor for the x-ray beam offset. Figures 14 and 15 also show that the high-current bunch has larger beam sizes than do the low-current bunches, likely due to its higher energy spread and the dispersions at the source point.

SUMMARY

The TCSPC technique has been used for bunch-by-bunch diagnostics of the stored beam in the APS storage ring. For bunch purity monitors, the new TDC and improved detector and electronics have made significant performance improvement possible. We demonstrated that it is possible to use TCSPC technique for measuring the longitudinal and transverse profiles. We note that significant improvement of resolution is not only possible but also probable as we test other hardware and software tools. For example, developing a proper treatment for the tails in the detector response curve would allow us to use detectors with better temporal resolution, thus improving the system resolution. We would like to thank Glenn Decker and Louis Emery for stimulating discussions for the interpretations of the data. We would also like to thank Om Singh for his strong support of bunch purity system upgrade.

REFERENCES

[1] O. V. Desmond, and D. Phillips, “Time-Correlated Single Photon Counting,” Academic Press, London, 1984.
[2] W. Becker, “Advanced Time-Correlated Single-Photon Counting Techniques,” Springer, Berlin, 2005.
[3] A.H. Lumpkin, C.-Y. Yao, B.X. Yang, and T. Toellner, “Bunch Purity Evolution During APS Storage Ring Top-up Operations,” PAC’03, p. 2411 (2003); http://www.JACoW.org.
[4] W. E. Norum and B. Yang, Eric Norum, “A Novel FPGA-based Bunch Purity Monitor System at the APS Storage Ring,” PAC’07, p. 4384 (2007); http://www.JACoW.org.
[5] Y. Kang, et al, “Dark Count Probability and Quantum Efficiency of Avalanche Photodiodes for Single-Photon Detection,” Appl. Phys. Lett., Vol. 83, p. 2955, 2003.
[6] Datasheet for id100, IDQ, www.idquantique.com.
[7] Datasheet for PicoHarp 300, PicoQuant GmbH, www.picoquant.com.
[8] Datasheet for PDM Series, Micro Photon Devices, www.microphotondevices.com.